Molecular Crystals and Liquid Crystals
Publication details, including instructions for authors and subscription information:
http://www.tandfonline.com/loi/gmcl16

# Exciton Sounding of α-Particle Induced Radiation Defects in Anthracene

S. Arnold [a] , H. T. Hu [a] & M. Pope [b]
[a] New York University, Radiation and Solid Laboratory
[b] New York University, Radiation and Solid State Laboratory and Chemistry Department
Version of record first published: 21 Mar 2007.

To cite this article: S. Arnold , H. T. Hu & M. Pope (1976): Exciton Sounding of α-Particle Induced Radiation Defects in Anthracene, Molecular Crystals and Liquid Crystals, 36:3-4, 179-192

To link to this article: http://dx.doi.org/10.1080/15421407608084322

*Mol. Cryst. Liq. Cryst.*, 1976, Vol. 36, pp. 179–192

Printed in Holland



# Exciton Sounding of α-Particle Induced Radiation Defects in Anthracene

S. ARNOLD, H. T. HU

*New York University, Radiation and Solid State Laboratory*

and

M. POPE

*New York University, Radiation and Solid State Laboratory and Chemistry Department*

(*Received June 2, 1976*)

Anthracene crystals have been irradiated ∥ to $c'$ by α-particles at 28.3, 30.00 and 32.26 MeV. A laser beam focused to a line ⊥ to the $c'$ direction is used to generate triplet excitons at 50 micron intervals in this direction. The spatial distribution of residual damage is determined from the variations in the delayed fluorescence and triplet exciton lifetime. The modulation of the triplet exciton lifetime in a magnetic field indicates that the defects are principally paramagnetic. The α-particle ranges at 30.00 and 32.26 MeV are 580 ± 20μ and 660 ± 20μ in agreement with the Bragg additivity rule. The $G$ value for the production of the paramagnetic defects is 0.02.

## I INTRODUCTION

The passage of heavy ions through solids produces long-lived defects. In organic solids such as anthracene some defects anneal at room temperature; however, most show no evidence of annealing.[1] These defects may be generally classified as either paramagnetic or nonparamagnetic. The spatial distribution of the defects is generally assumed to be proportional to the stopping power along the track. Neither the ratio of paramagnetic to non-paramagnetic defects nor the spatial distribution of these defects have been measured in organic crystals. The characterization of residual defects in organic matter is important for an understanding of the role which these defects play in the trapping of charge carriers and the quenching of excited states. In addition, due to the chemical similarities between biological

systems and organic crystals, and the sensitivity of biological systems to free radicals.[2] the determination of the spatial distribution of free radicals and the yield of these radicals is important in evaluating the effects of radiation therapy.

The ability of excitons to migrate in organic crystals may be used to detect radiation defects. For example, triplet excitons are readily quenched by free radicals[3] and mechanical defects.[4] This quenching can be detected by observing the changes in the delayed fluorescence produced by triplet–triplet fusion reactions. In addition, these two quenching interactions behave differently in a magnetic field; quenching by nonparamagnetic defects is unaltered in a magnetic field, whereas the quenching of triplet excitons by paramagnetic species is reduced in a magnetic field.[5] In the present study anthracene crystals were irradiated by monoenergetic α-particles at 28.3, 30.00 and 32.26 MeV. The spatial distribution of the radiation damage in these crystals was detected by observing the triplet exciton lifetime as a function of position from the point at which the α-particles entered the crystal. Delayed light was generated in small selective regions of the crystal by focusing laser excitation on the crystal. In order to determine the relative influence of paramagnetic and nonparamagnetic defects, the magnetic field effect on the triplet lifetime[5] was measured as a function of position.

## II THEORY

The basic kinetic equation governing the time dependence of a triplet exciton density $n(x, t)$ generated by an incident intensity $I(x, t)$ is given by

$$\frac{\partial n(x, t)}{\partial t} = \alpha I(x, t) - \beta n - \gamma_t n^2 + D \frac{\partial^2 n}{\partial x^2} \tag{1}$$

where $\alpha$ is the absorption constant for direct singlet to triplet absorption ($S_0 \rightarrow T_1$), $\beta$ is the monomolecular decay rate, $\gamma_t$ is the bimolecular decay rate, and $D$ is the exciton diffusion coefficient. In the present experiments, as we will verify in Section III, both the third and fourth terms on the right hand side of equation (1) are small compared with $\beta n$ so that when the excitation is cut-off the triplet density will decay exponentially with a time constant $1/\beta$. In the presence of both paramagnetic and nonparamagnetic defects, the rate constant $\beta$ may be written in terms of these contributions, as

$$\beta(H) = \beta_0 + \sum_{i=1}^{l} \gamma_{pi}(H) N_{pi} + \sum_{j=1}^{m} \gamma_{nj} N_{nj} \tag{2}$$

where $\beta_0$ is the intrinsic exciton rate constant, $\gamma_{pi}$ and $N_{pi}$ are the quenching rate and density of paramagnetic defects of the $i$th type, and, $\gamma_{nj}$ and $N_{nj}$ are

the quenching rate and density of nonparamagnetic defects of the $j$th type. The $H$ in parenthesis identifies the terms that are sensitive to the presence of an external magnetic field. As will be shown in Section V, all known paramagnetic quenching rates in anthracene are similar in magnitude and limited principally by diffusion. For this reason, equation (2) will be rewritten in terms of an average paramagnetic quenching rate $\bar{\gamma}_p$ and the total number of paramagnetic quenchers, $N_p$.

$$\beta(H) = \beta_0 + \bar{\gamma}_p(H)N_p + \sum_i^m \gamma_{ni} N_{ni} \tag{3}$$

Experimentally, $\beta$ is determined from the time constant of the decay of the delayed fluorescence (DF). This DF arises from bimolecular annihilation of triplet excitons and is proportional to the $\bar{\gamma}_t n^2$ term in equation (1). It can easily be shown that $\beta$ is half the rate constant for the decay of the delayed fluorescence.

The relative role of paramagnetic and nonparamagnetic defects may be determined in a magnetic field, since $\bar{\gamma}_p$ is reduced by the field and $\gamma_{ni}$ remains constant. The change in $\beta$ in the magnetic field, $\Delta_H\beta$, from equation (3) is therefore

$$\Delta_H\beta = (\Delta_H\bar{\gamma}_p)N_p \tag{4}$$

where $\Delta_H\bar{\gamma}_p$ is the change in the paramagnetic quenching rate. The ratio of the triplet decay constant in a magnetic field to that in the absence of a magnetic field is given by

$$\frac{\beta(H)}{\beta(0)} = \frac{\left[\dfrac{\Delta_H\bar{\gamma}_p}{\bar{\gamma}_p}\right]R}{\left[\dfrac{\beta_0}{\beta(0) - \beta_0} + 1\right]} + 1 \tag{5}$$

where

$$R = \left[1 + \frac{\sum \gamma_{nj} N_{nj}}{\bar{\gamma}_p N_p}\right]^{-1} \tag{6}$$

In the above equation $R$ represents the dilution in the magnetic field effect due to paramagnetic defects by nonparamagnetic defects. By fitting equation (5) to the magnetic field effect on the triplet lifetime, $(\Delta_H\bar{\gamma}_p/\bar{\gamma}_p)R$ may be determined. With a suitable value of $(\Delta_H\bar{\gamma}/\bar{\gamma}_p)$, $R$ may be estimated. The yield of paramagnetic defects per unit energy absorbed, $Y_p$, is then calculated from

$$Y_p = \frac{1}{F_\alpha E_\alpha \bar{\gamma}_p R^{-1}} \int_0^r \Delta_d\beta \, dx \tag{7}$$

where $F_\alpha$ is the total number of α-particles absorbed per unit target area, $E_\alpha$ is the incident energy of the α-particles, $x$ is the depth of penetration from the surface, $r$ is the range of penetration and $\Delta_d\beta$ is $\beta(0) - \beta_0$.

## III EXPERIMENTAL PROCEDURES

In this section we describe briefly the method of crystal preparation, of irradiation, and of radiation damage detection.

Highly purified crystals of anthracene were cleaved along the *ab* plane and oriented so that they could be cut repeatedly into 1 mm plates perpendicular to the *ab* plane along the *a* axis. The resulting *ac'* plates were typically 5 mm square. The crystals were polished to an optical finish on a benzene soaked lens tissue.

The irradiation was carried out at the Tandem Van de Graaff Facility of the Brookhaven National Laboratories. The α-particles were accelerated to energies of 30.00, 32,26, and 28.3 MeV; the number of α-particles absorbed were $(3.7 \pm 1.5) \times 10^8$, $(3.8 \pm 1.5) \times 10^8$ and $(1.0 \pm 0.4) \times 10^{12}$ $cm^{-2}$, respectively. The α-particles were directed along the $c'$ axis of the crystal. The average current from the accelerator was calculated by measuring the charge collected per unit time in a Faraday cup positioned behind the target volume without the crystal in place. The α-particle absorption per unit area was calculated by dividing the absorbed charge by the area of the 2 mm × 4 mm collimator directly upstream from the target. A mechanical chopper upstream from the sample was used to pulse the beam striking the sample for times varying from 4 msec to 56 sec. The overall charge entering the crystal was computed from the product of the pulse duration and the beam current. Due to possible beam inhomogeneity and beam intensity fluctuations, the uncertainty in the calculated flux is estimated to be ±40%. The experimental set-up for the irradiation is shown in Figure 1.

A diagram of the apparatus used to detect the radiation damage is shown in Figure 2. The radiation damage was detected by selective exciting portions

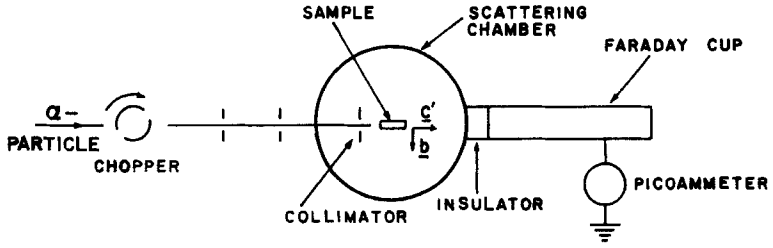


FIGURE 1 Experimental arrangement for heavy ion irradiation.

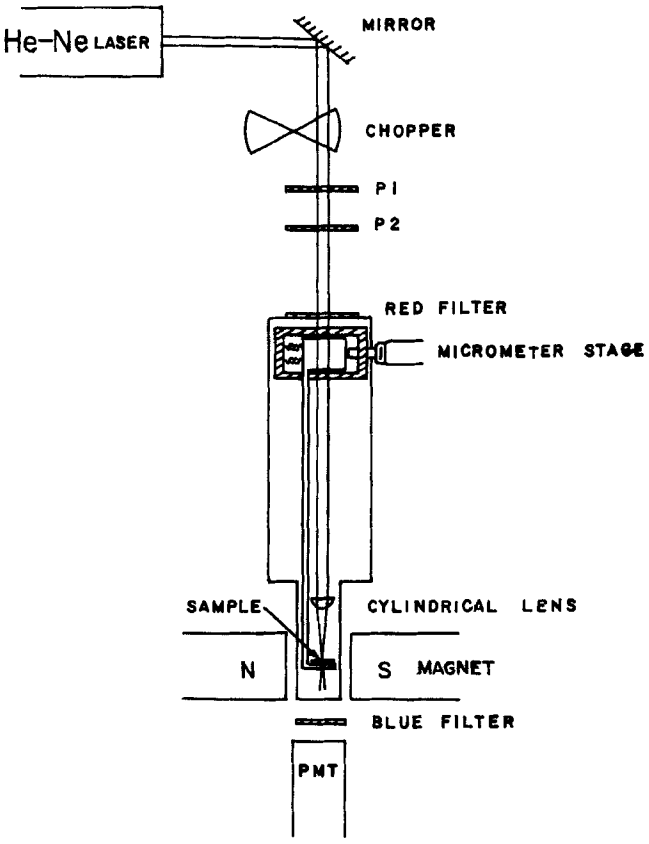


FIGURE 2 Apparatus used for detecting radiation damage.

of the crystals with a focused He–Ne laser beam. The laser beam was focused to a line by means of a cylindrical lens with a 51 mm focal length. The line of excitation found at the focal plane of the cylindrical lens was parallel to the crystal plate and perpendicular to the $c'$ axis. This geometry was used because triplet exciton diffusion in the $c'$ direction is at least an order of magnitude slower than in other directions so that distortions of the triplet exciton density due to this diffusion are thereby minimized. The crystal was moved along the $c'$ axis by means of a micrometer stage with a resolution of $10\mu$ per division. In order to eliminate the widening of the line of excitation due to birefringence, polarizer P2 was rotated so that its axis of polarization was parallel to one of the optical principal axes of the crystal. Polarizer P1 was used to attentuate the laser beam so that the steady-state luminescence was proportional to the square of the incident intensity. Under this condition the bimolecular term may be neglected in equation (1). The delayed

fluorescence produced from bimolecular annihilation of the triplet excitons was isolated by a blue filter combination (Corning CS-5-58 and CS-4-72) and detected by a photomultiplier. The single photon pulses from this photomultiplier were conditioned by an amplifier and discriminator and fed in parallel into a single scalar and a multichannel scalar. For steady-state measurements the scalar was gated on for 10 second intervals. Due to small fluctuations in the incident laser intensity with magnetic field, a photodiode followed by a current to frequency converter and a second scalar was used to record the incident intensity over the same period; the data were then normalized for fluctuations in this intensity. For transient lifetime measurements the multichannel analyzer was triggered to sweep synchronously with the chopper shown in Figure 2.

The magnetic field of 3000G was directed in the *ac* plane and magnetic field measurements were carried out on samples in which luminescence could be detected for all depths shallower than the Bragg peak.

The profile of the laser beam in the region of the focal plane was determined by measuring the light intensity distribution at the focal plane of the cylindrical lens with a photodiode preceeded by a $10\mu$ pinhole. A Gaussian shape was found at the skirt with a full width at half intensity of $30 \pm 8\mu$. Such a width is consistent with the theoretical diffraction limit[7] for a laser beam with a 0.6 mm effective aperture and therefore indicates that the measured width is diffraction limited. The influence of scattered light and crystal defects in broadening the skirt width within the crystal cannot be estimated in any simple way, however, since scattered light certainly exists, it is important to have at least an empirical method for estimating the total width of the excitation.

Levine *et al*[8] have shown that for excitation of width $d$ within a crystal, the delayed luminescence $F$ is given by

$$F = \frac{C}{d}\left\{1 - \left(\frac{3L}{2\sqrt{2}d}\right) + \exp\left(-\frac{\sqrt{2}d}{L}\right)\left[\left(\frac{\sqrt{2}L}{3d}\right) + \frac{1}{2}\right]\right\} \tag{8}$$

where $C$ is a constant and $L$ is the triplet exciton diffusion length. Since $d$ in our crystal is greater than $20\mu$ and $L$ is less than $5\mu$[6] the third term in the above expression can be neglected and

$$F \simeq \frac{C}{d}\left\{1 - \frac{3L}{2\sqrt{2}d}\right\}. \tag{9}$$

For the case of an unfocused laser beam of width $d_\infty$, $L/d_\infty \ll 1$ and the luminescence $F_\infty$ is

$$F_\infty = \frac{C}{d_\infty}. \tag{10}$$

The ratio $F/F_\infty$ is

$$\frac{F}{F_\infty} = \frac{d_\infty}{d}\left\{1 - \frac{3L}{2\sqrt{2}d}\right\} \tag{11}$$

and

$$d \simeq \frac{d_\infty F_\infty}{F} - \frac{3L}{2\sqrt{2}}. \tag{12}$$

Experiments with and without a cylindrical lens were performed and it was found that $F/F_\infty$ was about 8.5. Since $d_\infty$ in these experiments was measured to be 560$\mu$ and $L$ is known to be less that 5$\mu$,[6] the width of the laser excitation is calculated to be between 61 and 66$\mu$. Of course the precise distribution of excitons is not known. If this distribution is flat then the excitation and resolution widths will be identical. If, however, the exciton distribution is Gaussian in shape, the quadratic response of the luminescence will produce a lower limit for the resolution of 43$\mu$. In conclusion the resolution is no worse than 66$\mu$ and probably no better than 43$\mu$.

The effect of the diffusion term in equation (1) will be to increase the decay rate of the delayed light. Numerical calculations of the decay of the delayed fluorescence using a focused laser beam with 50$\mu$ width indicate that the perturbation of the lifetime of the luminescence is much smaller than the effect due to defects. For example, for a triplet lifetime of 20 msec and the upper limit on the diffusion coefficient of $1.5 \times 10^{-5}$ cm$^2$/sec,[6] the increase in the decay rate of the delayed fluorescence due to diffusion will be about 4%. In the damaged area where the triplet lifetime is no larger than 3 msec, this perturbation will be less than 2%.

## IV EXPERIMENTAL RESULTS

Figure 3 shows the exciton decay rate, $\beta(0)$, as a function of position from the irradiated surface for samples irradiated at 30.00 and 32.26 MeV. These rate constants were calculated from the fastest decay rate that could be expressed as a single exponential. Due to the width of the focused laser beam, and the rapidly changing spatial distribution of defects within 50$\mu$ of the Bragg peak, the delayed fluorescence decays became highly nonexponential in this region. Outside of this resolution limit, the decays were exponential over at least two and one-half time constants. Unfortunately since the laser intensity profile is not known within the crystals, the decays were not deconvoluted for the width of the laser excitation. For this reason, the data can only be considered to be an accurate indication of the defect concentration beyond 50$\mu$ from the

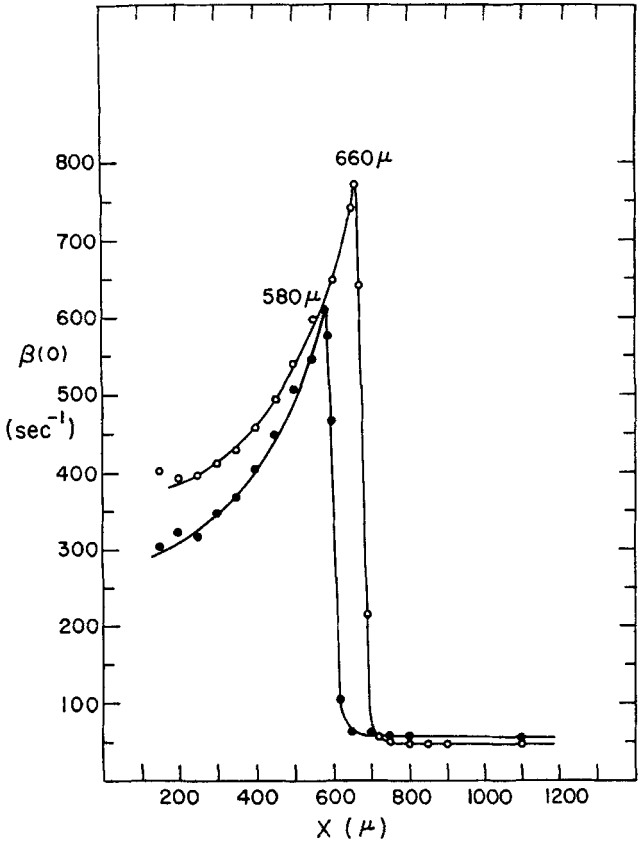


FIGURE 3 Triplet decay rate constant $\beta(0)$ versus depth $X$ in microns, $\mu$. –○– irradiated at 32.26 MeV; –●– irradiated at 30.00 MeV. The number of $\alpha$-particles absorbed at 32.26 MeV and 30.00 MeV were $(3.8 \pm 1.5) \times 10^8$ cm$^{-2}$ and $(3.7 \pm 1.5) \times 10^8$ cm$^{-2}$, respectively. The particle current densities at 32.26 MeV and 30.00 MeV were $(8.5 \pm 3.4) \times 10^8$ cm$^{-2}$-s$^{-1}$ and $(3.4 \pm 1.3) \times 10^{10}$ cm$^{-2}$-s$^{-1}$.

Bragg peak. As one can see in Figure 3 no data were taken at depths of 0 to 100$\mu$ since surface scattering in this region produced highly nonexponential decays. The position of the Bragg peaks at 30.00 and 32.26 MeV were established by noting the depth at which there was a minimum in steady-state delayed fluorescence intensity; these were found to be at $590 \pm 20\mu$ and $670 \pm 20\mu$, respectively. These points were also in correspondence with the points at which the decay rate was found to undergo a maximum. The profiles shown in Figure 3 were measured one hour after irradiation and no substantial changes were found in these profiles over the next five months.

The steady-state luminescence $L$ can be shown from equation (1) to be proportional to $\gamma_t \alpha^2/\beta^2$, where $\alpha$ is the $S_0 \rightarrow T_1$ absorption coefficient.

Measurements of the steady-state luminescence $L$ were also made as a function of penetration depth in order to see whether $\beta$ was the only parameters affected by the radiation. The values of $L\beta^2$ were found to be relatively independent of position up to within $50\mu$ from the Bragg peak. This constancy of $L\beta^2$ indicates that only $\beta$ is affected by the irradiation, consistent with the model proposed in Section II.

Figure 4 shows the spatial variation of $(\beta(0) - \beta_0)$ for a crystal irradiated at 28.3 MeV with a substantially higher dose, $10^{12}$ cm$^{-2}$, than was used for the crystals in Figure 3 (see Section III). Experimentally no luminescence could be observed within the estimated Bragg peak for this sample. The calculated range of $\alpha$-particles at 28.3 MeV is $532\mu$. The profile shown in Figure 4 was measured 24 hours after the irradiation and no substantial changes from these values were noted within a period of one year. The exponential tail in Figure 4 has a characteristic decay length of $227\mu$. Other crystals irradiated at 27 MeV with doses of the order of $10^{12}$ cm$^{-2}$ revealed similar tails. The lack of tails in the 30.00 and 32.26 MeV irradiations is most likely the result of the small radiation doses used in these experiments and the uncertainty of $\pm 0.5$ sec$^{-1}$ in the triplet rate constant measurements.

The magnetic field effect $\beta(H)/\beta(0)$ at a depth of $350\mu$ was measured in the 32 MeV sample for $H \| ac$. The magnitude of this effect is similar to measurements made by Ern and Merrifield[5] for anthracene irradiated by x-rays. Resonances were found at angles of $20 \pm 3$ and $74 \pm 3$ degrees to either side

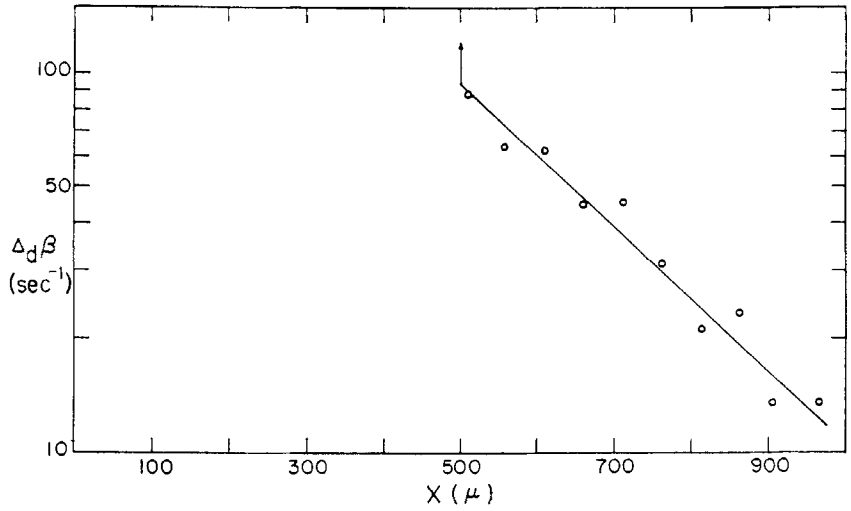


FIGURE 4 The change in triplet exciton decay rate constant after irradiation, $\Delta_d\beta$ versus depth for the sample irradiated at 28.3 MeV with an absorbed dose and a particle current density of $(1.0 \pm 0.4) \times 10^{12}$ cm$^{-2}$ and $1.78 \times 10^{10}$ cm$^{-2}$-s$^{-1}$, respectively.

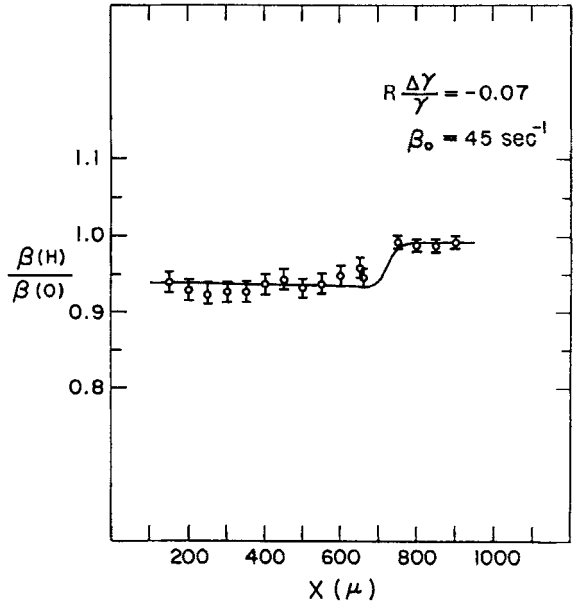


FIGURE 5 Ratio of triplet exciton decay rate constant in the presence of a magnetic field $H$, to that in the absence of a magnetic field, $\beta(H)/\beta(0)$ as a function of depth $X$ in microns. The solid line represents the fit to equation (5) with $R\Delta_H\bar{\gamma}_p/\bar{\gamma}_p = -0.07$ and $\beta_0 = 45\ s^{-1}$.

of the $a$ axis in agreement with theory.[5] The "on" resonance and "off" resonance values of $\beta(H)/\beta(0)$ were found to be $0.935 \pm 0.010$ and $0.980 \pm 0.010$, respectively. The spatial dependence of $\beta(H)/\beta(0)$ at the "on" resonance position is illustrated in Figure 5. As one can see $\beta(H)/\beta(0)$ remains close to 0.94 from $100\mu$ to $650\mu$ and increases to $0.990 \pm 0.007$ beyond $750\mu$.

## V DISCUSSION

The results in Figure 3 may be compared with theoretical estimates for the stopping power [linear energy transfer (LET)] of anthracene, $-(dE/dx)$. The spatial stopping power profile in anthracene may be estimated from the stopping power of carbon and hydrogen[9] by the Bragg additivity rule. According to this rule the stopping power of a compound is the sum of the stopping powers of its constituents. The calculated stopping power profiles and the triplet rate constant profiles are compared in Figure 6. The ranges of 30.00 MeV and 32.26 MeV of $662\mu$ and $582\mu$ are in good agreement with the experimental values of $660 \pm 20\mu$ and $580 \pm 20\mu$. Since the experimental resolution of $\sim 50\mu$ is large compared with the $12\mu$ halfwidth of the Bragg

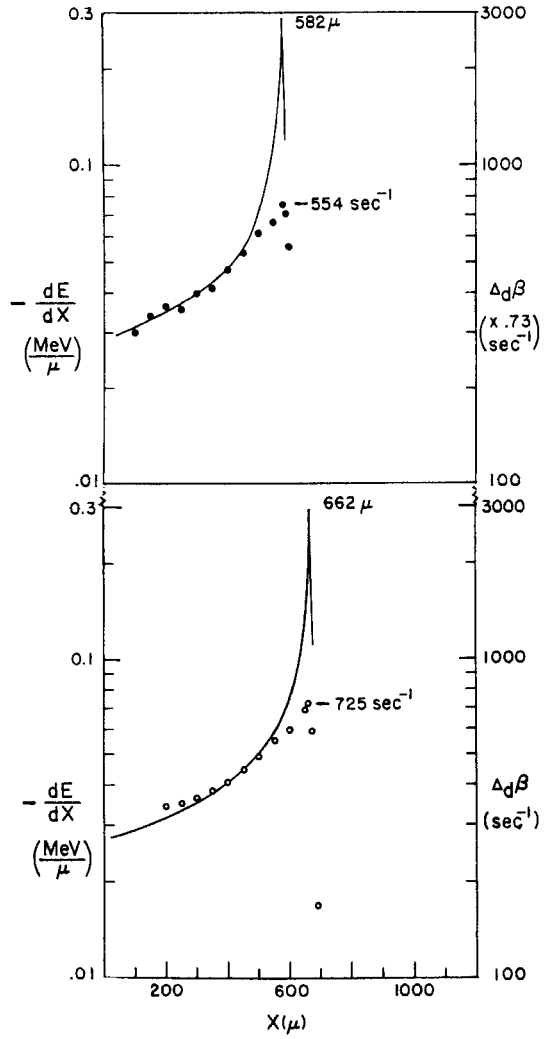


FIGURE 6 Comparison of spatial distribution of simulated stopping power $(-(dE/dx))$ and triplet exciton decay rate change $\Delta_d\beta$. -○- irradiated at 32.26 MeV; -●- irradiated at 30.00 MeV.

peak, the actual damage at the Bragg peak is not measured. However, at depths less than the position of the Bragg peak minus $\sim 50\mu$ a comparison between the simulation and the damage profile should be reasonable. As one can see the agreement is quite good within $80\mu$ of the peak. In the case of an initial energy of 30.00 MeV, the LET at a depth of $80\mu$ above the Bragg peak corresponds to a particle residual energy of 10 MeV. We can therefore

say that the damage is proportional to the stopping power from 32 MeV to 10 MeV. If we assume that the damage is also proportional to the absorbed dose per unit area $F_\alpha$, which is reasonable since Co $\gamma$ experiments[3] show such a proportionality with more than one hundred times the change in triplet rate constant found in the present experiments, then we may write

$$\Delta_d \beta = B_\alpha F_\alpha \left(\frac{dE}{dx}\right) \tag{13}$$

where $B_\alpha$ in equation (13) is the amount by which the triplet decay rate is changed for each erg/cm$^3$ of energy absorbed. For the crystals irradiated at 30.00 and 32.00 MeV, $B_\alpha$ is found to be $(1.3 \pm 0.5) \times 10^{-3}$ and $(1.6 \pm 0.6) \times 10^{-3}$ sec$^{-1}$ – cm$^3$/erg. These values are consistent within their uncertainties even though the irradiation at 30.00 MeV was carried out at 34 times the particle current density used at 32.26 MeV. This correspondence indicates that the influence of bimolecular processes in the formation of the defects is relatively unimportant below particle current densities of $3 \times 10^{10}$ cm$^{-2}$ – s$^{-1}$. In addition the values of $B_\alpha$ in these experiments are close to the value of $B_\alpha$ of $1.2 \times 10^{-3}$ s$^{-1}$ – cm$^3$/erg obtained by Ern and McGhie[10] in their experiments dealing with internal irradiation by 18 KeV $\beta$-particles produced by the decay of tritium.

According to Burton *et al*,[11] the energy loss events in a track can be relatively far apart, (such as is the case when high energy electrons pass through matter) producing a low LET track, or the loss events can occur in close proximity (such as the case when $\alpha$-particles pass through matter) producing a high LET track. The high LET portions of the track, representing the energy loss events themselves, are referred to as short tracks and blobs by Burton *et al.*[11] These authors point out that when chemical changes occur as a result of radiation absorption, the extent of these changes is roughly proportional to the fraction of the energy deposited in the form of short tracks and blobs. In the case of irradiation with 18 KeV $\beta$-particles produced by radioactive decay of tritium, Burton *et al* estimates that about 60% of the energy is deposited in the form of short tracks and blobs. It thus appears that the 18 KeV electrons produce a high LET track and the agreement between the results of Ern and McGhie[10] and of this paper confirm this conclusion.

The magnetic field effect shown in Figure 5 may be fit to equation (5) by using the data in Figure 3. The fit shown in Figure 5 requires a value of $R\Delta_H \bar{\gamma}_p/\bar{\gamma}_p$ of $-0.07$. Within experimental error, this value is almost identical to the value obtained by Ern and Merrifield[5] in their study of defect production in anthracene by x-rays. Ern and McGhie[10] have shown that such a magnetic field effect indicates a simple situation with only paramagnetic

centers, and therefore $\Delta_H \bar{\gamma}_p/\bar{\gamma}_p \simeq -0.07$ and $R \simeq 1$. With this estimate of $R$ the yield of paramagnetic defects may be calculated from equation (6).

By substituting equation (13) into equation (7) with $R = 1$, we have

$$Y_p = \frac{1}{E_\alpha \bar{\gamma}_p} \int_0^r B_\alpha \, dE. \tag{14}$$

In terms of the average value of $B_\alpha$, $\bar{B}_\alpha = [\int_0^r B_\alpha \, dE]/E_\alpha$, the yield in equation (14) reduces to $\bar{B}_\alpha/\bar{\gamma}_p$. Since $B_\alpha$ has been shown to be constant over the first 68% of the energy loss and the next 32% of the energy loss is not expected to change the value of $\bar{B}_\alpha$ significantly, $\bar{B}_\alpha$ will be taken as the average value for the two samples: $1.4 \times 10^{-3}$ sec$^{-1}$ cm$^3$ erg$^{-1}$. The quenching rate of triplet excitons by paramagnetic radiation defects, $\bar{\gamma}_p$, has not been reported; however, its value may be estimated from luminescence and EPR measurements. Blum *et al*[12] have reported that Co $\gamma$ produces $10^{17}$ spins per cm$^3$ for a dose of $10^7$ r. Weisz *et al*[3] have reported the increase of the triplet decay rate constant for this same radiation to be $1.1 \times 10^{-1}$ sec$^{-1} - r^{-1}$. Therefore the rate constant for quenching, which is the change in $\beta$ per spin/cm$^3$ is $1.3 \times 10^{-11}$ cm$^3$-sec$^{-1}$. This number is in close agreement with the quenching rate of $7 \times 10^{-12}$ cm$^3$-sec$^{-1}$ for triplets by trapped holes,[13] which are also paramagnetic. This correspondence implies that the quenching process is limited principally by diffusion. In anthracene such rates are typically $\sim 10^{-11}$ cm$^3$/sec. Taking $\bar{\gamma}_p = 10^{-11}$ cm$^3$/sec in equation (14), the yield of paramagnetic species for $\alpha$-particle irradiation in the energy range from 32 MeV to 10 MeV is found to be $1.4 \times 10^8$/erg. The G value for the production of these paramagnetic defects is approximately 0.02.

The precise reason for the long tail shown in Figure 4 is not well understood. However, certain possibilities may be ruled out. The damage caused by the following should not reach far enough in the region of the tail.

a) Carbon $K_\alpha$ x-rays

b) Carbon recoils

c) Secondary electrons

Other mechanisms may not be ruled out in terms of range. These damage mechanisms are:

d) Recoiled protons

e) Channelled $\alpha$ particles and secondary protons

f) Bremsstrahlung from secondary electrons, $\alpha$-particles and secondary protons

g) $\gamma$-radiation arising from resonance excitation of the carbon nucleus.

Some slower mechanisms may also be important. Of these, molecular diffusion along grain boundaries and line defects is known to be fast from self-diffusion studies[14] and may allow paramagnetic species, such as the radiation defects, to alter their distributions between the time of irradiation and measurement. In addition, both α-particles and secondary protons may be channelled into the region beyond the Bragg peak. The influence of such factors as channelling and diffusion may not be easily estimated although the others are amanable to calculation. Experiments are under way to ascertain the principle mechanism for the long tail in the defect density profile.



## Acknowledgements

We would like to thank the members of the Tandem Van DeGraaff Group at the Brookhaven National Laboratory for making available to us the accelerator facility used in this work. We would also like to thank Professor N. E. Geacintov at New York University and Dr. C. E. Swenberg at the National Institute for Mental Health in Washington, D.C. for their useful suggestions. This work was supported by the Energy Research and Development Administration.

## References

1. J. Levinson, J. Marrero, A. Cobas, and S. Z. Weisz, *J. Lum.* **1, 2**, 726 (1970).
2. H. B. Demopoulos, *Federation Proc.* **32**, 1859 (1973).
3. S. Z. Weisz, P. Richardson, and A. Cobas, *Mol. Cryst.* **4**, 277 (1968).
4. S. Arnold, W. B. Whitten, and A. C. Damask, *J. Chem. Phys.* **53**, 2878 (1970).
5. V. Ern and R. E. Merrifield, *Phys. Rev. Lett.* **21**, 609 (1968).
6. V. Ern, *Phys. Rev. Lett.* **22**, 343 (1969).
7. The full width at half maximum at the skirt of a focused laser beam operating in a $TEM_{0,0}$ mode is $\lambda f \ln 4/(\pi a)$; $\lambda$, $f$ and $a$ are respectively the wavelength, focal length and aperture (full width at half intensity). For the present set-up this equation gives a width of 24$\mu$.
8. M. Levine, J. Jortner, and A. Szöke, *J. Chem. Phys.* **45**, 1591 (1966).
9. L. C. Northcliffe and R. F. Schilling, *Nuc. Data Tables* **A7**, 233–463 (1970).
10. V. Ern and A. R. McGhie, *Mol. Cryst. and Liq. Cryst.* **15**, 277 (1971).
11. M. Burton, K. Funabashi, R. R. Hentz, P. K. Ludwig, J. L. Magee and A. Mozumder in *Transfer and Storage of Energy by Molecules*, Vol. I, John Wiley and Sons Ltd., London and New York, p. 161 (1969).
12. H. Blum, P. L. Mattern, R. A. Arndt, and A. C. Damask, *Mol. Cryst.* **3**, 269 (1967).
13. V. Ern, H. Bouchriha, J. Fourny, and G. Delacote, *Solid State Comm.* **9**, 1201 (1971).
14. J. N. Sherwood in *Surface Defects and Properties of Solids*, Vol. 2, The Chemical Society (Benlington House, London), p. 250 (1972).